2012

Observation and simulation of winds and hydrodynamics in St. Johns and Nassau Rivers

Peter Bacopoulos
University of Central Florida, peter.bacopoulos@ucf.edu

Scott C. Hagen
University of Central Florida

Andrew T. Cox
Oceanweather, Inc.

William R. Dally
Surfbreak Engineering Sciences, Inc.

Steven Bratos
United States Army Corps of Engineers

Journal of Hydrology 420–421 (2012) 391–402

Contents lists available at SciVerse ScienceDirect

Journal of Hydrology

journal homepage: www.elsevier.com/locate/jhydrol

Observation and simulation of winds and hydrodynamics in St. Johns and Nassau Rivers

Peter Bacopoulos [a,*], Scott C. Hagen [a], Andrew T. Cox [b], William R. Dally [c], Steven M. Bratos [d]

[a] University of Central Florida, Department of Civil, Environmental, and Construction Engineering, 4000 Central Florida Blvd., P.O. Box 162450, Orlando, FL 32816, USA
[b] Oceanweather, Inc., 5 River Road, Suite 1, Cos Cob, CT 06807, USA
[c] Surfbreak Engineering Sciences, Inc., Winter Park, FL 32792, USA
[d] United States Army Corps of Engineers, Water Resources Engineering Branch, 701 San Marco Blvd., P.O. Box 4970, Jacksonville, FL 32232, USA

ARTICLE INFO

Article history:
Received 4 March 2011
Received in revised form 26 November 2011
Accepted 17 December 2011
Available online 23 December 2011
This manuscript was handled by Konstantine P. Georgakakos, Editor-in-Chief, with the assistance of Vincent S. Neary, Associate Editor

Keywords:
Tides
River flows
Storm event
Sea level anomaly
Manning's roughness

SUMMARY

Water surface elevations and daily flows are measured in the St. Johns and Nassau Rivers (north Florida) and reveal a storm event in mid-May 2009 and a sea level anomaly in June and July 2009. In an effort to reproduce these events, wind and tidally driven hydrodynamics are simulated from the deep ocean into the St. Johns and Nassau Rivers using a shallow water equations model. Calibration adjusts spatially distributed Manning's roughness based on modeled-observed discharge. For validation, the model captures the regular tidal fluctuation as well as the hydrodynamic responses of the storm event in mid-May at the six water level gaging stations. At the flow gaging station, the model captures the ebb tendency of the tide as well as a strong perturbation (flood pulse) that occurs because of the storm event in mid-May.

1. Objective and purpose

The objective and purpose is twofold: to further establish the capability of shallow water equations models as prognostic tools of estuarine and riverine circulation over longer term records (on the order of months); and to elucidate the hydrodynamics that occur in the St. Johns and Nassau Rivers under calm conditions (when tides are predominant) and during storm events (when tides act in the presence of winds and atmospheric pressure changes).

2. Domain description

The South Atlantic Bight (SAB) coast is laden with estuaries and inland waterways (Dame et al., 2000). From the larger scale perspective, the SAB is situated within the western North Atlantic Ocean. Discrete representation of the SAB, including all estuarine water bodies and intertidal zones, is provided (Bacopoulos et al., 2011). The boundary of the SAB model extends over and beyond the continental shelf and Blake's Plateau. Boundary forcings are derived from the Western North Atlantic Tidal (WNAT) model domain (Hagen et al., 2006), which includes the western North Atlantic Ocean, Gulf of Mexico, and Caribbean Sea (Fig. 1a).

The SAB finite element mesh applied herein (Fig. 1b) was constructed semi-manually by digitizing, first, the estuarine water bodies, and second, the intertidal zones (Bacopoulos et al., 2011). A bathymetric–topographic dataset was assembled, conformed to the North American Vertical Datum (NAVD88) and interpolated to the mesh nodes using a locally linear interpolation scheme. Bathymetry data sources included recent surveys of the main channel (United States Army Corps of Engineers Jacksonville District, 2011) and historical surveys of the river tributaries (National Oceanic and Atmospheric Administration, 2011). Topographic data sources included LIDAR-derived terrain elevations (Camp Dresser & McKee Inc., 2007).

The region of interest comprises the St. Johns and Nassau Rivers, located in north Florida (Fig. 1c and d). The St. Johns River is the longest river (500 km) contained wholly within Florida and drains a watershed covering approximately 22,000 km^2. The bathymetric profile is near flat (slope = 0.000022) which allows tidal effects to extend at least 170 km upriver (Toth, 1993). Located just north of the St. Johns River is the Nassau River which drains a watershed of 1100 km^2 (Ayres Associates, 1999). The land cover of the region is characterized by low-lying coastal plains and tidal marshes to the east and forested wetlands and uplands to the west.

* Corresponding author. Tel.: +1 407 823 1176; fax: +1 407 823 3315.
E-mail address: peter.bacopoulos@ucf.edu (P. Bacopoulos).

0022-1694/$ - see front matter © 2011 Elsevier B.V. All rights reserved.
doi:10.1016/j.jhydrol.2011.12.032

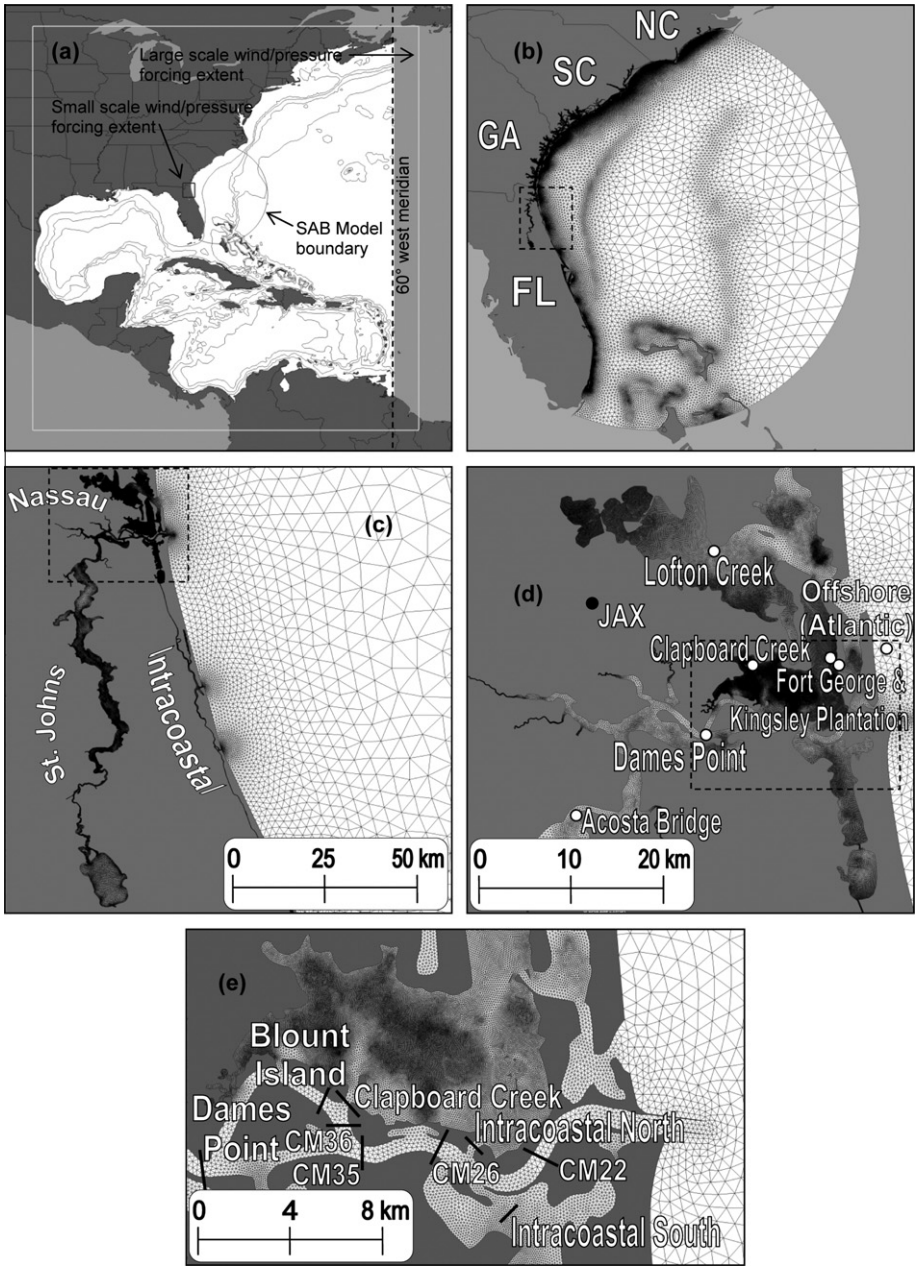

Fig. 1. (a) Western North Atlantic Tidal model domain with contour lines drawn for 183-, 1200-, 2500-, and 4500-m isobaths, (b) South Atlantic Bight mesh, (c–e) insets of St. Johns and Nassau Rivers, Atlantic Intracoastal Waterway, and intertidal zones, including six hydrodynamic measurement locations (○) and nine cross sections (—). JAX stands for Jacksonville International Airport.

3. Record of interest

The time period of interest is May 1–July 31, 2009. This 3-month period includes a storm event in mid-May as well as a sea level anomaly in June and July. The storm event in mid-May is evident in the wind record (National Climatic Data Center, 2011) available for Jacksonville International Airport (JAX) (see Fig. 1d for location and Figs. 2 and 3 for wind speeds and directions, respectively). The sea level anomaly of June and July 2009 is documented (Sweet et al., 2009) as being the result of perigean spring tide conditions, northeasterly wind forcing, and dynamical setup by the Florida Current. Generally, such events (storm or extreme tide) cause increased flooding around the coast and along the St. Johns and Nassau Rivers. Storm events can also cause significant currents, capable of causing bottom or bridge pier scour.

4. Measured hydrodynamics

Hydrodynamic measurements include time series of water surface elevations at six coastal stations located inside (five) and offshore (one) the St. Johns and Nassau Rivers and time series of daily flows at a river station located 60 km upstream in the St. Johns (Fig. 1d). The five coastal stations located inside the St. Johns and Nassau Rivers are named Fort George, Kingsley Plantation, Clapboard Creek, Dames Point, and Lofton Creek. The offshore station is named Offshore (Atlantic) and the river station is named Acosta Bridge.

Measured water surface elevations at the six coastal stations are provided by Surfbreak Engineering Sciences, Inc. (2009) and are displayed in Figs. 4–9. Note that the tide gauge for Offshore (Atlantic) does not average samples onboard but instead reports

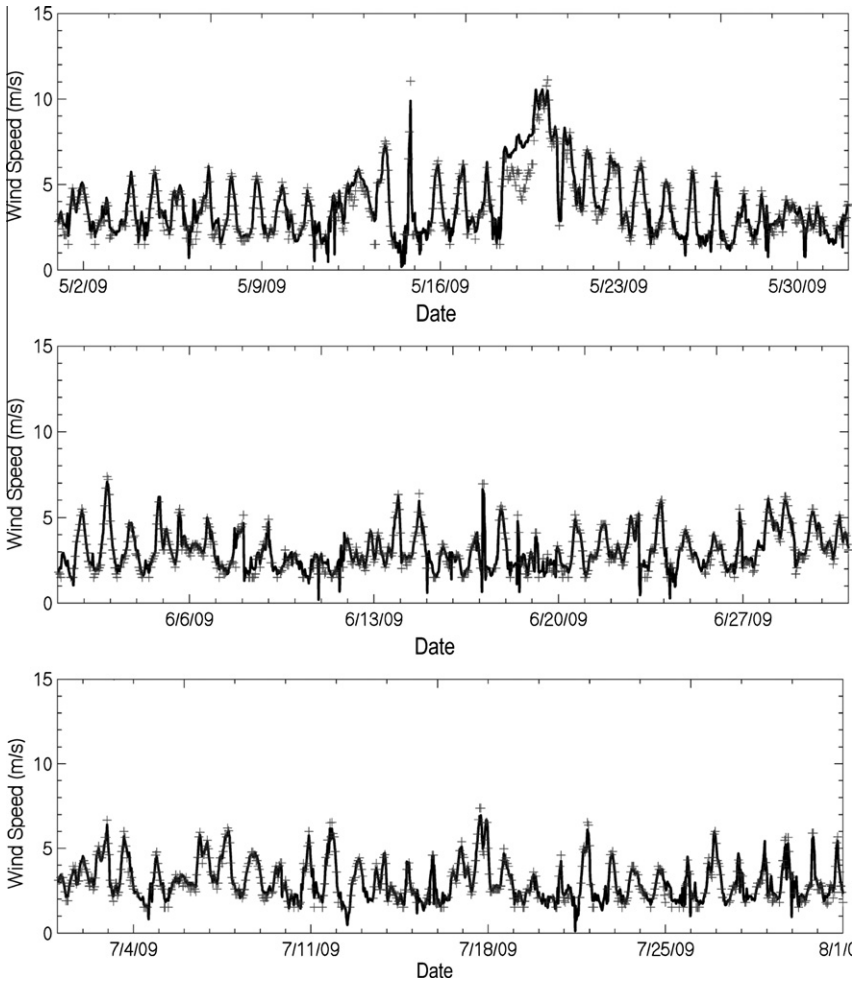

Fig. 2. Wind speeds (m/s) at Jacksonville International Airport: measured (+) and National Center for Environmental Protection Global Forecast System (−).

instantaneous pressures that include wave heights, which is the explanation for the relatively noisy signal at this location (Fig. 4). All six coastal stations exhibit a surge (1–1.5 m above NAVD88) during the storm event in mid-May. Additionally, there is a subtle setdown of 0.5 m during the first 10 days of May, evident in the record for the stations that were active during that time. The sea level anomaly of June and July 2009 is exhibited most noticeably in the latter part of June 2009 in the form of increased water surface elevations (+0.25 m) coupled with large tidal ranges (2–3 m). Lastly, there appears to be some non-astronomic tide behavior in the third week of July.

Measured daily flows at the river station are provided by the United States Geological Survey (2010) and are displayed in Fig. 10. Positive flow values represent flow downriver and negative flow values represent flow upriver. For the most part, daily flows are downriver. It is also known that tributary inflows can contribute to the downriver flow (Bergman, 1992). The negative spike ($-1500\ m^3/s$) and subsequent rebound ($+1500\ m^3/s$) in mid-May are correlated with the 5–10 m/s wind event (out of the north–northeast) that persisted from May 19th to the 21st (Figs. 2 and 3). After the rebound, it took one week for flow to subside to $1000\ m^3/s$ and three weeks to subside to $500\ m^3/s$.

5. Modeled wind and atmospheric pressure fields

Wind speeds and atmospheric pressures are computed using the Interactive Objective Kinematic Analysis (IOKA) system (Cox et al., 1995) where tropical storm winds from a re-analysis performed using the H∗Wind system (Powell et al., 1998) and local measurements are blended into a synoptic-scale wind and atmospheric pressure field provided by the National Center for Environmental Protection Global Forecast System (NCEP GFS) (National Weather Service, 2011). A tropical model, hereafter referred to as TC96 (Thompson and Cardone, 1996), governed by vertically integrated equations of motion that describe horizontal airflow through the planetary boundary layer (Cardone et al., 1994), is applied to each tropical system within the model domain providing atmospheric pressure fields to complement the IOKA/H∗Wind wind fields. TC96 calculates snapshots (in time) that represent distinct phases of the storm's evolution and is driven by the National Hurricane Center/Tropical Prediction Center track and intensity information as well as by data obtained from hurricane hunter aircraft and analyzed by the Hurricane Research Division Wind Analysis System (Powell et al., 1998).

Local wind measurements from six land stations, including Jacksonville International Airport (see Fig. 1d for location), and one Coastal-Marine Automated Network (C-MAN) station are assimilated into the IOKA system to provide local-scale wind response over the St. Johns and Nassau Rivers. Figs. 2 and 3 display the time histories of wind speeds and directions at Jacksonville International Airport compared to the NCEP GFS winds before IOKA assimilation. A large-scale wind and atmospheric pressure forcing that extends over the entire WNAT model domain utilizes IOKA assimilation on an analysis grid with 28-km spacing. A small-scale

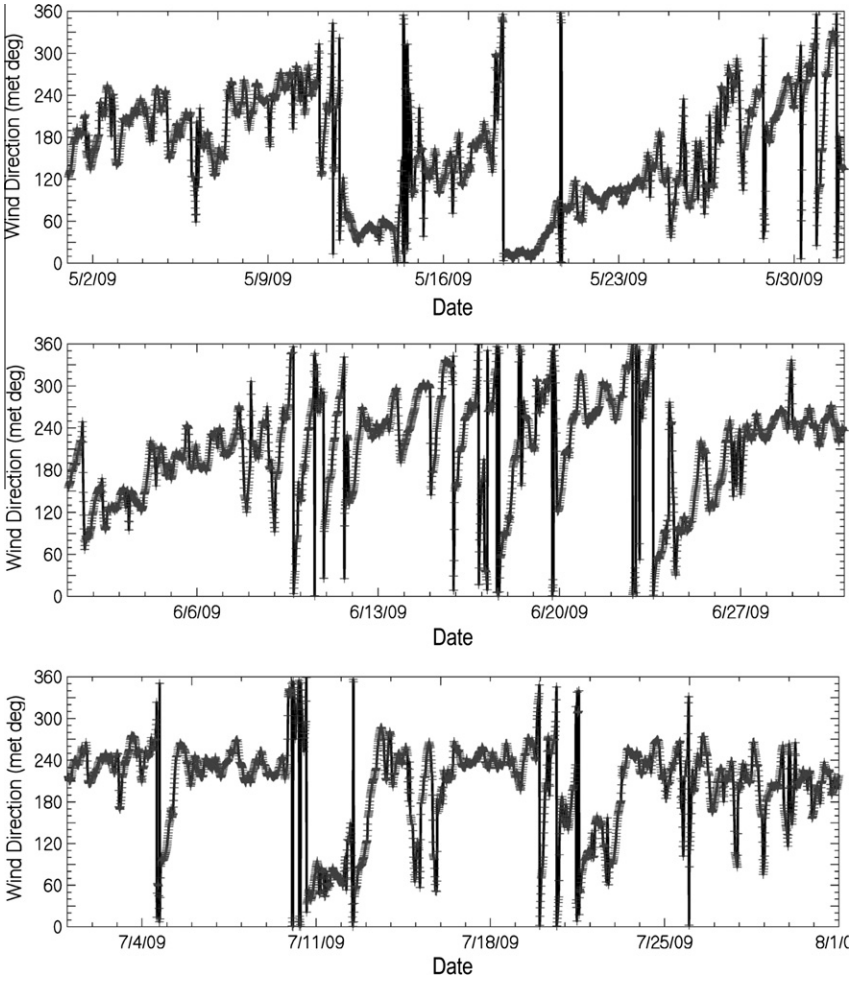

Fig. 3. Wind directions (°) at Jacksonville International Airport: measured (+) and National Center for Environmental Protection Global Forecast System (—).

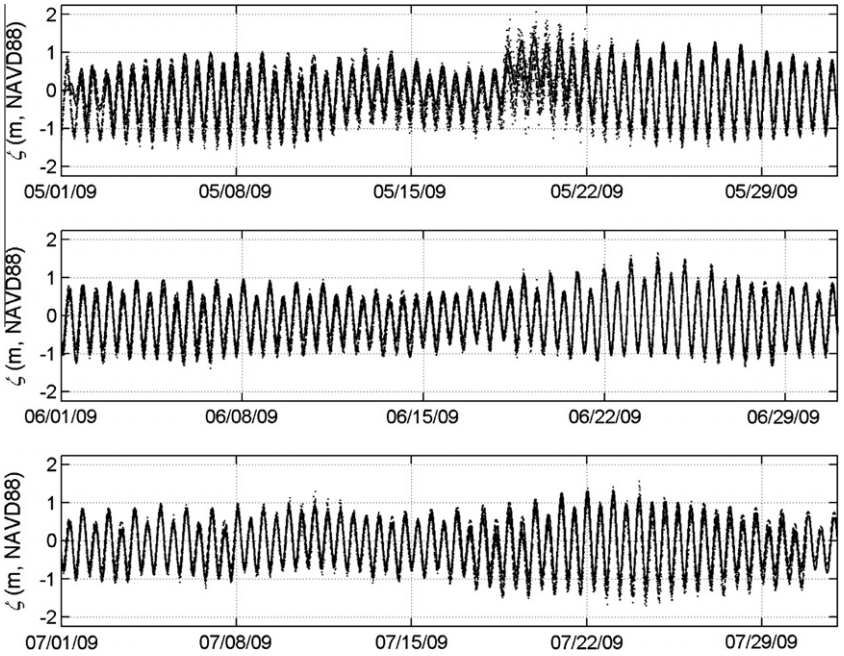

Fig. 4. Validation plots: observed (●) water surface elevations and modeled tides only (– –) and tides with winds and atmospheric pressures (—) at offshore (Atlantic).

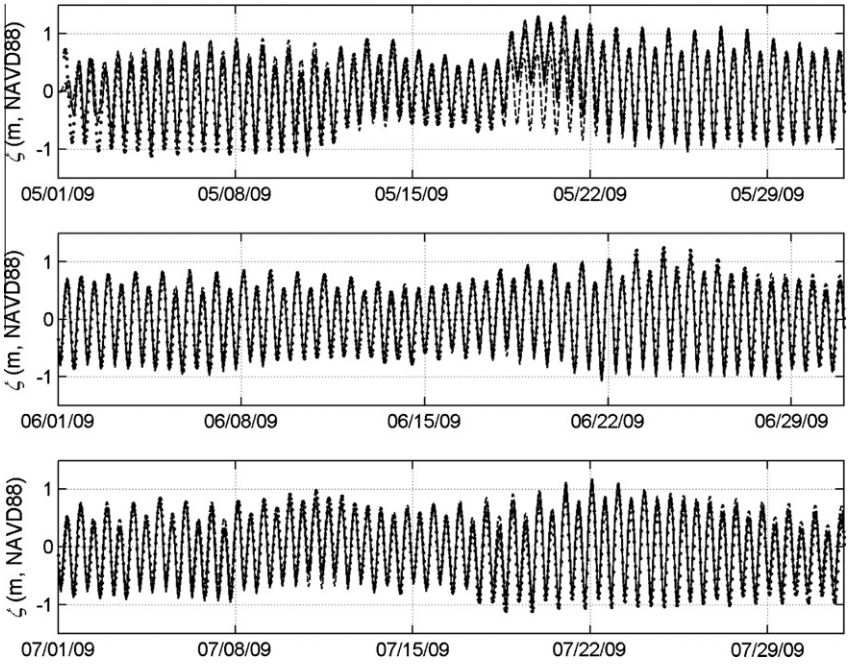

Fig. 5. Validation plots: observed (●) water surface elevations and modeled tides only (– –) and tides with winds and atmospheric pressures (—) at Kingsley Plantation.

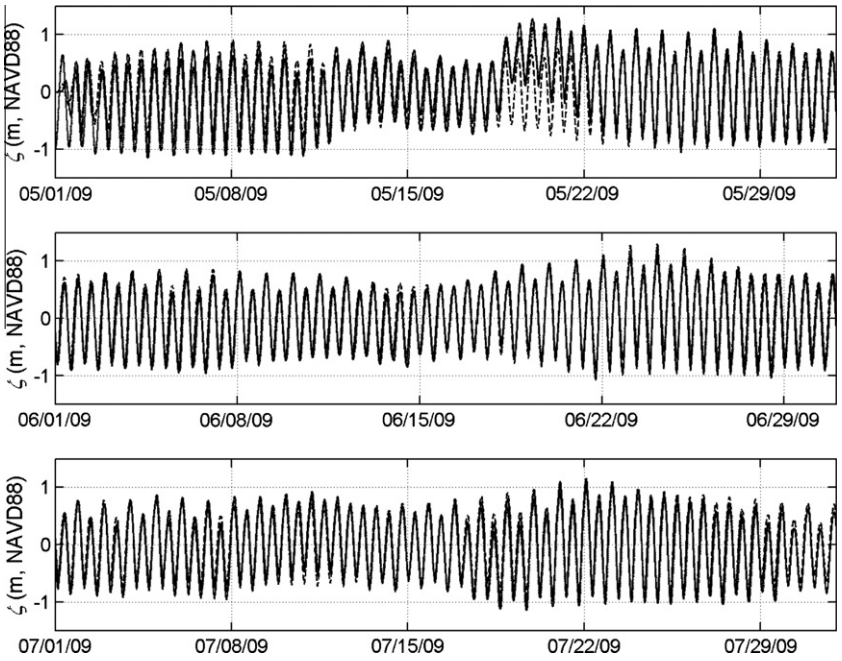

Fig. 6. Validation plots: observed (●) water surface elevations and modeled tides only (– –) and tides with winds and atmospheric pressures (—) at Fort George.

wind and atmospheric pressure forcing that extends over the St. Johns and Nassau Rivers utilizes IOKA assimilation on an analysis grid with 2.8-km spacing. During the interpolation of wind speeds and atmospheric pressures to the mesh nodes, the small scale forcing takes precedence over the large scale forcing. This nesting of the wind and atmospheric pressure forcing is illustrated in Fig. 1a.

6. Shallow water equations model

Hydrodynamic calculations are performed using the two-dimensional version of the ADvanced CIRCulation (ADCIRC) coastal ocean model (Luettich and Westerink, 2006b).

6.1. Governing equations and numerical methods

ADCIRC solves the shallow water equations (Kinnmark, 1985) in the form of the generalized wave continuity equation (GWCE) (Lynch and Gray, 1979; Kolar et al., 1994). A continuous Galerkin finite element scheme is applied over linear triangles in space and a three-level implicit scheme is used to propagate the solution forward in time (Westerink et al., 2008).

6.2. Model Parameterization and Settings

Bottom boundary friction is parameterized in ADCIRC as (Luettich and Westerink, 2006a):

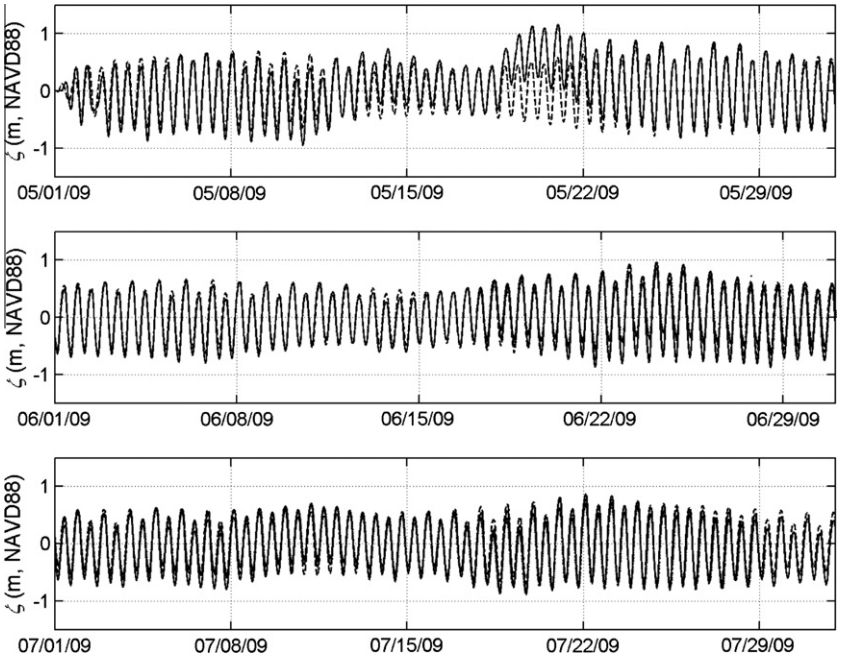

Fig. 7. Validation plots: observed (●) water surface elevations and modeled tides only (– –) and tides with winds and atmospheric pressures (—) at Dames Point.

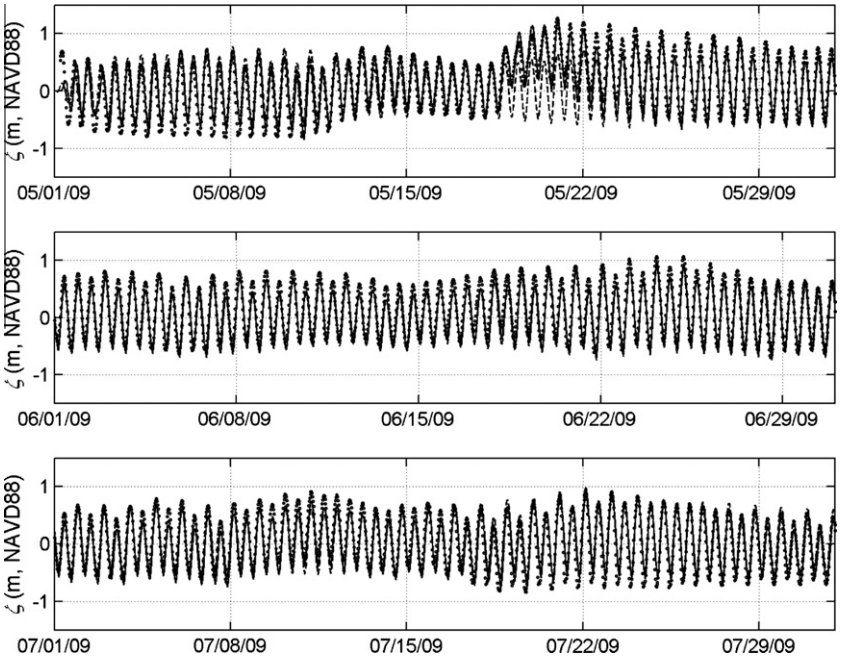

Fig. 8. Validation plots: observed (●) water surface elevations and modeled tides only (– –) and tides with winds and atmospheric pressures (—) at Clapboard Creek.

$$\tau_* = C_f\sqrt{U^2+V^2}/H \quad \text{and} \quad C_f = gn^2/H^{1/3} \tag{1}$$

where τ_* is bottom stress term (s^{-1}), C_f is bottom boundary friction coefficient (–), U and V are depth-integrated velocities (longitudinal and latitudinal directions, respectively) ($m\ s^{-1}$), H is total water column height (m), g is acceleration due to gravity ($m\ s^{-2}$), and n is Manning's roughness coefficient ($s\ m^{-1/3}$).

Manning's n values are specified as nodal attributes in the model (Luettich and Westerink, 2006b) based on spatial distributions of three land cover classes (those with tidal exposure) derived from the National LandCover Database 2001 (Homer et al., 2004): 'open water;' 'emergent herbaceous wetlands;' and 'woody wetlands.' Six tidal simulations are performed using different combinations of the spatially distributed Manning's n values (Table 1) to calibrate the model. The six scenarios are selected to cover the following range of Manning's n values: 0.015–0.030 for 'open water;' 0.035–0.065 for 'emergent herbaceous wetlands;' and 0.075–0.125 for 'woody wetlands.' These values are related to bed characteristics and are within ranges based on empirical data (Arcement and Schneider, 1989) and numerical experiments (Mattocks et al., 2006).

Model parameters, initialization, and boundary conditions used are provided in Table 2. The wetting and drying algorithm within ADCIRC (Dietrich et al., 2006) is enabled. The minimum bathymetric

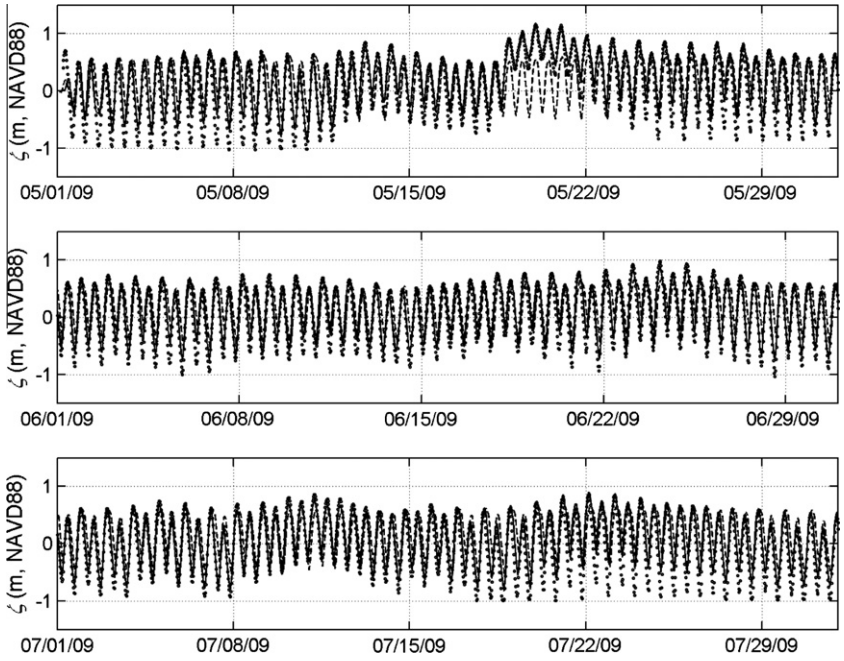

Fig. 9. Validation plots: observed (●) water surface elevations and modeled tides only (– –) and tides with winds and atmospheric pressures (—) at Lofton Creek.

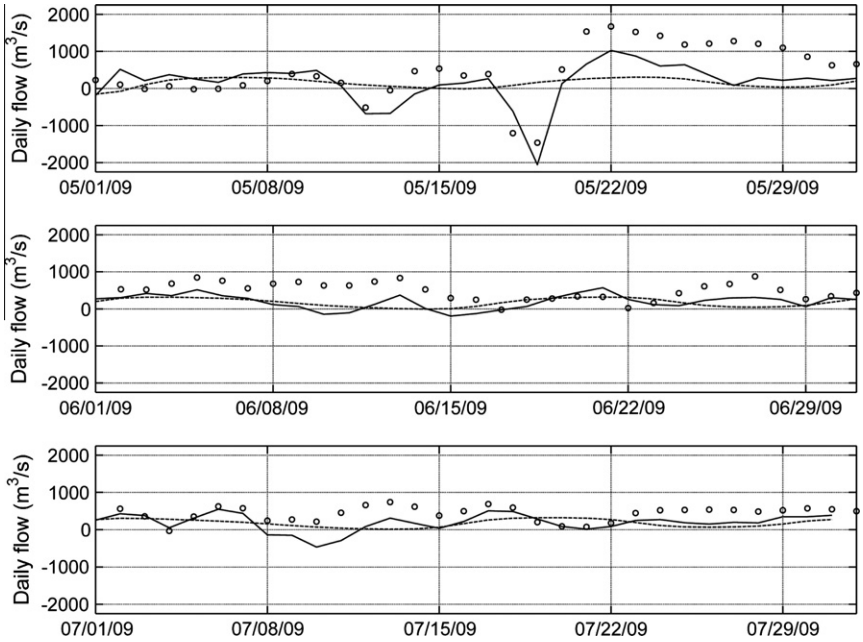

Fig. 10. Validation plots: observed (○) daily flows and modeled tides only (– –) and tides with winds and atmospheric pressures (—) at Acosta Bridge.

Table 1
Calibration runs: six tidal simulations using different combinations of spatially distributed Manning's *n* values.

Simulation	Manning's *n* per land cover class		
	'Open water'	'Emergent herbaceous wetlands'	'Woody wetlands'
Range of values	0.015–0.030	0.035–0.065	0.075–0.125
1	0.025 (mid-range)	0.050 (mid-range)	0.100 (mid-range)
2	0.030 (upper limit)	0.065 (upper limit)	0.125 (upper limit)
3	0.015 (lower limit)	0.035 (lower limit)	0.075 (lower limit)
4	0.015 (lower limit)	0.065 (upper limit)	0.125 (upper limit)
5	0.025 (mid-range)	0.035 (lower limit)	0.075 (lower limit)
6	0.025 (mid-range)	0.065 (upper limit)	0.125 (upper limit)

depth is set equal to 0.1 m, i.e., computational nodes and the accompanying elements with water depths less than the minimum bathymetric depth are considered to be dry. The minimum velocity which will permit flow to propagate into a dry element is set equal to 0.01 m/s. The advective terms are enabled. Horizontal eddy viscosity is set equal to 5.0 m^2/s (Bunya et al., 2010). The GWCE weighting parameter τ_0, which weights the relative contributions of the primitive-continuity and pure-wave forms of the GWCE (Lynch and Gray, 1979; Kolar et al., 1994), is set equal to $\tau_0 = 0.005$ when the water column height $H \geqslant 10$ m and $\tau_0 = 0.020$ when the water column height $H < 10$ m (Luettich and Westerink, 2006a). The model is setup to simulate a total of 92 days using a time step of 2 s. The simulation is initialized using a cold start (static equipotential surface). Boundary conditions (detailed in the following sub-sections) are ramped up over the first 7 days of the simulation.

6.3. Tidal boundary conditions

Boundary conditions for the WNAT model domain consist of: an elevation forcing along the 60° west meridian; and no normal flow (free tangential slip) along all coastlines. The elevation forcing is composed of seven principal tidal constituents (in order of decreasing amplitude: M2, S2, N2, K1, O1, K2, and Q1) interpolated from the global tidal model of Le Provost et al. (1998). Tidal potentials (Reid, 1990) associated with these same seven constituents are applied over the interior of the domain.

6.4. Atmospheric forcing functions

Surface stresses are computed using the formulation of Garratt (1977):

$$\frac{\tau_s}{\rho_w} = \frac{\rho_a V_{10}^2 C_D}{\rho_w} \quad \text{and} \quad C_D = \frac{\mu}{1000}(0.75 + 0.067 V_{10}) \tag{2}$$

where ρ_w is the density of seawater (kg m^{-3}), ρ_a is the density of air (kg m^{-3}), V_{10} is the wind speed acting 10 m above the surface (m s^{-1}), C_D is the wind speed-dependent drag coefficient (–), and μ is a multiplier set equal to 1.3 (Hagen et al., 2011) to convert the 30-min sustained winds to 10-min sustained winds (–).

Atmospheric pressure forcing is applied in the model as an inverted barometer effect which transforms the atmospheric pressure deficit (in stress units) into equivalent water column heights: $\zeta^p = (p_{\text{bar}} - p)/\rho_w g$, where ζ^p is the equivalent water column height (m), p_{bar} is the ambient atmospheric pressure (1013 hPa), p is the local atmospheric pressure (hPa), ρ_w is the density of seawater (kg m^{-3}), and g is acceleration due to gravity (m s^{-2}).

Atmospheric forcing is applied over the interior of the domain as temporally interpolated between 30-min snapshots of the modeled wind speeds and atmospheric pressures.

6.5. Hydrograph boundary conditions

Boundary conditions for the SAB model consist of: an elevation forcing along the open-ocean boundary that extends over and beyond the continental shelf and Blake's Plateau; and no normal flow (free tangential slip) along all coastlines. The elevation forcing comprises a hydrograph as extracted from simulation using the WNAT model domain. This nesting of the SAB model within the WNAT model domain is illustrated in Fig. 1a, which permits for capture of the remote effects of the winds (Bacopoulos et al., 2009).

7. Modeled hydrodynamics

Calibration runs consist of six tidal simulations that test model sensitivity with respect to spatially distributed Manning's roughness (Table 1). Validation runs consist of two numerical experiments utilizing the Manning's roughness that performed best in the calibration. The two experiments are: (i) with singular forcing using tides only; and (ii) with combined forcing using tides, winds, and atmospheric pressures. Note that the calibration time period (various dates in 1995–1997; see Fig. 11 for example) is different from the validation time period (May 1–July 31, 2009; see Fig. 10 for example).

Comparisons are made between simulated and measured water surface elevations and flows. For qualitative assessment, plots of water surface elevations and flows are used. For quantitative assessment, root mean square (RMS) errors are calculated: $\sqrt{\Sigma(x_{\text{sim}} - x_{\text{obs}})^2/N}$, where x_{sim} and x_{obs} are simulated and observed hydrodynamic variables (water surface elevations or flows) and N is the total number of data points.

7.1. Calibration

Calibration is based on six tidal simulations that use different combinations of the spatially distributed Manning's n values (Table 1). Observed data are available for four different dates (Sucsy and Morris, 2002): August 23, 1995; August 6, 1996; September 17, 1996; and September 22, 1997. The data records consist of discharge measurements, each covering one complete tidal cycle (approximately 12 h) for one or more of the four different dates, for nine cross sections in the St. Johns River (Fig. 1e). This permits for a total of fifteen model-data comparisons (Table 3). Simulated discharge is reconstructed using model output and the continuity equation:

$$Q = VA. \tag{3}$$

where Q is streamflow (m s^{-3}), V is simulated velocity (along-channel vector component) (m s^{-1}), and A is cross-sectional area (m^2). Note that the observations are the full response of the flow (tides, winds, inflows, etc.) whereas the simulations are of tides only. This is the primary reason for the poor fit in the model-data comparisons.

Table 2
Model parameters, initialization, and boundary conditions.

Name	Notation	Setting
Minimum bathymetric depth	h_0	0.1 m
Minimum wetting velocity	V_{min}	0.01 m/s
Advection	–	Enabled
Horizontal eddy viscosity	ν_T	5 m^2/s
Generalized wave continuity equation	τ_0	0.005 (if $H \geqslant 10$ m)
Weighting parameter		0.020 (if $H < 10$ m)
Run length	–	92 days
Time step	Δt	2 s
Initial conditions	–	Cold start (equipotential surface)
Boundary conditions	–	Tides (+ winds + atmospheric pressures)
Forcing ramp	–	7 days

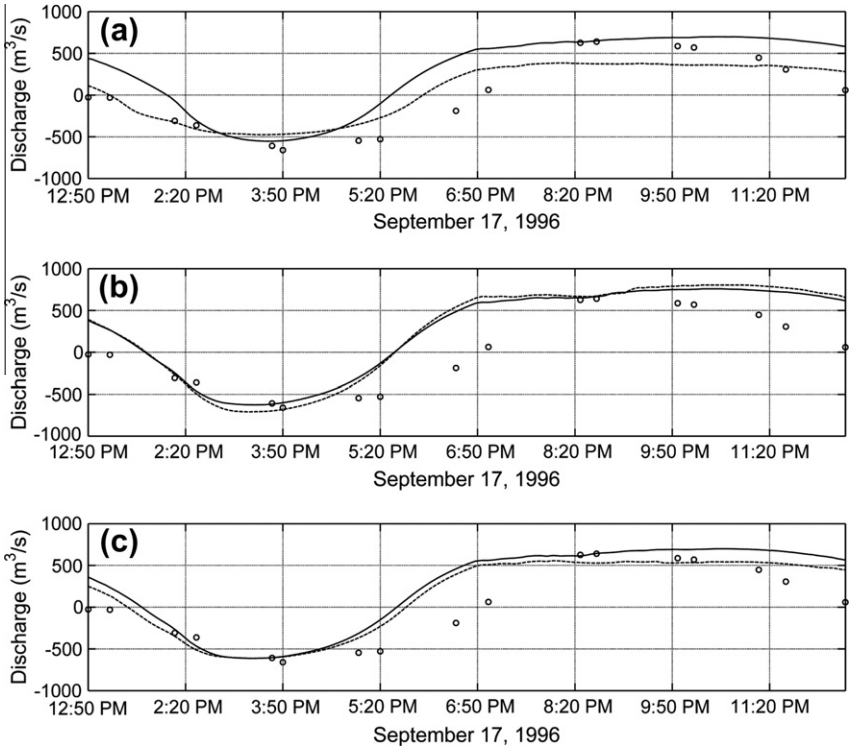

Fig. 11. Calibration plots: observed (○) and modeled (tides only) discharge at Clapboard Creek for (a) simulations 1 (—) and 2 (– –), (b) simulations 3 (—) and 4 (– –), and (c) simulations 5 (—) and 6 (– –).

Fig. 11 shows a plot of measured and simulated discharge for the cross section at Clapboard Creek. Regardless of the applied Manning's roughness, the model captures the range in discharge (−500 to +500 m^3/s) as well as the tidal phase (±1 h). There are some differences between the model curves; however, these results are the most sensitive of all obtained. Note that Clapboard Creek is directly hydraulically connected to the intertidal zones. The sensitivity is mostly attributed to bottom boundary friction setting in the intertidal zones.

RMS errors are reported in flow units (m^3/s) and as normalized values (100% × flow units ÷ peak flow) (Table 4). For each of the fifteen comparisons, the greatest difference (max error minus min error) is calculated among the six tidal simulations and quantifies model sensitivity. The error analysis demonstrates that Clapboard Creek is the most sensitive (20%) but also shows that there is appreciably less sensitivity at the other cross sections (2–14%). The sixth simulation ('open water' = 0.025, 'emergent herbaceous wetlands' = 0.065, and 'woody wetlands' = 0.125) has the lowest normalized RMS error (19% on average). On average, there is low model sensitivity (±8%) with adjustment of bottom boundary friction within ranges of physical meaning, as derived from land cover. With respect to any spatial variability, model sensitivity is greater in and around the intertidal zones relative to that found in fully wetted areas.

Table 3
Calibration approach: fifteen comparisons for one or more of four different dates for nine cross sections in Lower St. Johns River.

Comparison	Cross section	Date
1	Dames point	August 23, 1995
2	Dames point	August 6, 1996
3	Dames point	September 17, 1996
4	Dames point	September 22, 1997
5	Blount Island	September 17, 1996
6	Clapboard Creek	September 17, 1996
7	Channel Marker 36 (CM36)	August 6, 1996
8	Channel Marker 35 (CM35)	August 23, 1995
9	Channel Marker 35 (CM35)	September 22, 1997
10	Channel Marker 26 (CM26)	September 22, 1997
11	Intracoastal North	August 6, 1996
12	Intracoastal South	August 6, 1996
13	Channel Marker 22 (CM22)	August 23, 1995
14	Channel Marker 22 (CM22)	August 6, 1996
15	Channel Marker 22 (CM22)	September 22, 1997

7.2. Validation

Validation runs consist of two numerical experiments utilizing the Manning's roughness that performed best in the calibration. The two experiments are: (i) singular forcing using tides only; and (ii) combined forcing using tides, winds, and atmospheric pressures.

Note that the environment was relatively unchanged between the calibration time period (1995–1997) and the validation time period (2009). For the St. Johns and Nassau Rivers, changes in land cover were primarily related to urban development. The natural landscapes of the estuarine environment can be considered to have remained constant over the 12–14 year period between 1995/1997 and 2009, as determined by comparison of land use/land cover data (National Land Cover Data, 2011), i.e., 1992 dataset vs. 2001 dataset vs. 2006 dataset. We justify using the Manning's n distribution that performed best in the calibration for the validation runs on the basis of little environmental change, and thus of the land cover, over the time period between calibration and validation.

7.2.1. Qualitative assessment (plots)

Simulated water surface elevations are plotted against the measurements for the six coastal stations (see Fig. 1d for locations) in Figs. 4–9. First, winds and atmospheric pressures in addition to tides are effective in the model towards simulating water surface elevations. Both the 'tides only' and 'tides with winds and atmospheric

Table 4
Calibration results: root mean square errors (m^3/s, %) computed for fifteen comparisons based on six tidal simulations using different Manning's n distributions. Final column is greatest difference Δ (max error minus min error) calculated among simulations for each comparison.

Comparison	Simulation						
	1	2	3	4	5	6	Δ
1	411, 14	499, 17	422, 14	483, 16	410, 14	405, 14	94, 3
2	690, 17	801, 20	675, 17	722, 18	648, 16	680, 17	153, 4
3	884, 22	1195, 30	880, 22	911, 23	890, 22	804, 20	391, 10
4	638, 16	691, 17	628, 16	666, 17	617, 15	621, 16	74, 2
5	194, 13	193, 13	170, 11	246, 16	157, 10	128, 9	118, 8
6	330, 44	203, 27	331, 44	356, 47	304, 41	206, 27	153, 20
7	461, 26	396, 23	445, 25	359, 21	431, 25	333, 19	128, 7
8	586, 15	700, 18	605, 15	566, 14	586, 15	552, 14	148, 4
9	882, 16	1201, 22	772, 14	859, 16	752, 14	926, 17	449, 8
10	1010, 17	1247, 21	991, 17	993, 17	972, 16	1032, 17	275, 5
11	154, 34	160, 36	196, 44	205, 46	140, 31	163, 36	65, 14
12	412, 55	434, 58	418, 56	411, 55	423, 56	417, 56	23, 3
13	555, 10	971, 18	657, 12	1241, 23	631, 11	573, 10	686, 12
14	623, 11	856, 16	609, 11	623, 11	569, 10	523, 10	333, 6
15	785, 10	1221, 16	795, 11	738, 10	772, 10	755, 10	483, 6
Average	574, 21	718, 23	573, 22	625, 23	553, 20	541, 19	238, 8

pressures' simulations capture the tidal phase (±1 h) and range (1–3 m); however, only the 'tides with winds and atmospheric pressures' simulation captures the surge (1–1.5 m above NAVD88) during the storm event in mid-May as well as the subtle setdown (−0.5 m) during the first 10 days of May.

Second, the spring-neap (fortnightly) tidal cycle and the lunar-based monthly variation are exhibited in the model output (Figs. 4–9). Neap (minimum) tide range is approximately 1 m and spring (maximum) tide range is 2–3 m. The model also captures the large tidal ranges (2–3 m) associated with sea level anomaly of June and July 2009.

Third, the model captures the damping of the tide, i.e., the diminishing of the range when going upriver (Figs. 4–9). To quantify tidal decay, maximum tidal ranges are compared at the six coastal stations. Offshore (Atlantic) (representative of the shelf/ocean tide) has a maximum tidal range of 3 m; Kingsley Plantation and Fort George (located 10 km upriver in Fort George) have a maximum tidal range of 2 m; Lofton Creek (located 30 km upriver in Nassau) has a maximum tidal range of 1.75 m; and Dames Point and Clapboard Creek (located 30 km upriver in the St. Johns) have a maximum tidal range of 1.5 m. By this, the tide decays by ⅓ over the lower 10 river km and by ½ over the lower 30 river km.

Simulated daily flows are plotted against the measurements for the river station (see Fig. 1d for location) in Fig. 10. Simulated daily flows are reconstructed using model output and the continuity equation (Eq. (3)). The resulting time series are then averaged every 24 h to generate daily flows that can be compared with the measurements.

First, the model captures the ebb tendency of the tide as reflected in the data record (Fig. 10). This is evidenced by the generally positive flow values (0–333 m^3/s) generated by the 'tides only' simulation that compares to the positive flow values (0–750 m^3/s) in the observed data during calm conditions, e.g., in June and July. Note that tributary inflows, which are not included in the model, provide a baseline (downriver) flow (Bergman, 1992). This is the primary reason for the under-prediction in the magnitude of the daily flows.

Second, the flow reversal (flood pulse) that occurs during the storm event in mid-May is exhibited in the model output (Fig. 10). This is evidenced by the negative spike (−2000 m^3/s) generated by the 'tides with winds and atmospheric pressures' simulation, which compares to the negative spike (−1500 m^3/s) in the observed data, as well as by the subsequent rebound (+2000 m^3/s) generated by the 'tides with winds and atmospheric pressures' simulation, which compares to the subsequent rebound (+1500 m^3/s) in the observed data. The timing of the negative spike and rebound are on the mark, but the magnitude of the negative spike is over-predicted and the magnitude of the rebound is under-predicted. In addition, the data show the flow after the rebound to be attenuated over three weeks until it subsided. However, this attenuation of the flow is not fully captured in the model. The over-prediction of the negative spike, under-prediction of the rebound, and partial (not full) capture of the flow attenuation are attributed to the absence of tributary inflows in the model. Tributary inflows would oppose the flood pulse resulting in a lower magnitude of the negative spike, would reinforce the rebound to result in a higher magnitude of the flow, and would attenuate the flow in the weeks following the rebound.

7.2.2. Quantitative assessment (RMS errors)

RMS errors are reported in linear or flow units (cm or m^3/s) and as normalized values (100% × linear or flow units ÷ peak water surface elevation or peak flow) for the 'tides only' and 'tides with winds and atmospheric pressures' simulations (Table 5). The second and third columns are the RMS errors for the entire 3-month data record (May 1–July 31, 2009); the fourth and fifth columns are for May 18–25 (storm event); and the sixth and seventh columns are for the entire data record excluding May 18–25 (calm conditions).

With respect to water surface elevations, the 'tide with winds and atmospheric pressures' simulation outperforms the 'tides only' simulation (Table 5). In assessing the entire 3-month data record, the RMS errors are lower, on average, by approximately 22% in the 'tides with winds and atmospheric pressures' simulation relative to the 'tides only' simulation (18 vs. 23 cm). In assessing the storm event (May 18–25), RMS errors are lower, on average, by over 50% in the 'tides with winds and atmospheric pressures' simulation relative to the 'tides only' simulation (19 vs. 45 cm). Even for calm conditions, the 'tide with winds and atmospheric pressures' simulation outperforms the 'tides only' simulation (18 vs. 20 cm).

With respect to daily flows, the 'tide with winds and atmospheric pressures' simulation outperforms the 'tides only' simulation (Table 5). In assessing the entire 3-month data record, the RMS errors are lower by approximately 22% in the 'tides with winds and atmospheric pressures' simulation relative to the 'tides only' simulation (434 vs. 557 m^3/s). In assessing the storm event (May 18–25), the RMS errors are lower by over 45% in the 'tides with winds and atmospheric pressures' simulation relative to the 'tides only' simulation (653 vs. 1200 m^3/s). Even for calm conditions,

Table 5
Validation results: root mean square errors (second and third columns) for entire 3-month data record (May 1–July 31, 2009), (fourth and fifth columns) May 18–25 (storm event), and (sixth and seventh columns) entire data record excluding May 18–25 (calm conditions). 'T' stands for 'tides only' and 'TWP' stands for 'tides with winds and atmospheric pressures.'.

Station	Entire data record		'Storm event'		'Calm conditions'	
	T	TWP	*T*	TWP	*T*	TWP
Root mean square error (water surface elevations) (cm, %)						
Offshore (Atlantic)	30, 20	25, 17	46, 31	37, 25	26, 17	25, 17
Kingsley Plantation	24, 19	17, 14	47, 38	13, 10	20, 16	17, 14
Fort George	23, 18	17, 14	42, 34	12, 10	19, 15	18, 14
Dames Point	16, 13	16, 13	–[a]	–[a]	16, 13	16, 13
Clapboard Creek	21, 17	17, 14	46, 37	17, 14	17, 14	17, 14
Lofton Creek	25, 20	17, 14	44, 35	14, 11	21, 17	17, 14
Average	23, 18	18, 14	45, 36	19, 15	20, 16	18, 14
Root mean square error (daily flows) (m^3/s, %)						
Acosta Bridge	557, 37	434, 29	1200, 80	653, 44	444, 30	396, 26

[a] Cannot be computed due to lack of data.

the 'tide with winds and atmospheric pressures' simulation outperforms the 'tides only' simulation (396 vs. 444 m^3/s).

8. Summary and conclusions

Wind and tidally driven hydrodynamics are observed and simulated in the St. Johns and Nassau Rivers over a 3-month time period, May 1–July 31, 2009. The record includes a storm event in mid-May and a sea level anomaly in June and July. Hydrodynamics are simulated using a shallow water equations model of the South Atlantic Bight and associated estuaries and intertidal zones to recreate observed water surface elevations and daily flows.

Calibration adjusts spatially distributed Manning's roughness based on modeled-observed discharge. The calibration indicates that there is low model sensitivity with adjustment of bottom boundary friction within ranges of physical meaning, as derived from land cover. As well, model sensitivity is not spatially uniform but is instead greater in and around the intertidal zones than in open water bodies. This follows the intuition that shallower flows experience higher relative resistance from bottom boundary friction.

The model is validated utilizing the Manning's n distribution that performs best in the calibration. Model solutions are compared to the observations for two numerical experiments: one that employs forcing of tides only; and the other that employs forcing of tides plus winds and atmospheric pressures. The following conclusions result: (i) hydrodynamics in the St. Johns and Nassau Rivers are tidally dominated but are also sensitive to wind forcing; (ii) while water surface elevations in the coastal region are primarily the response of tides and winds, daily flows upstream are a combined response of coastal dynamics (due to tides and winds) and hydrology (due to watershed runoff); (iii) winds become important during storm events, as is the case of mid-May 2009, but can also contribute during calm conditions, as is the case with the subtle setdown from May 1st to the 10th; (iv) tides generally predominate and at times can be excessive in range, as is the case of the sea level anomaly of June and July 2009; (v) daily flows in the St. Johns and Nassau Rivers are almost always flowing downriver, driven mainly by hydrologic inflows, but are reinforced by the ebb-dominance of the tide; and (vi) winds can drive reversals in daily flows. On this latter point, winds capable of reversing daily flow need not necessarily be of tropical storm or hurricane force. In fact, winds from typical frontal systems can cause flow reversals, as occurs in the 3-month time period (May 1–July 31, 2009) examined herein.

This study demonstrates the utility of a shallow water equations model as a prognostic tool of estuarine and riverine circulation over a longer term (monthly scale) record. Future hydrodynamic studies in the St. Johns and Nassau Rivers should apply wind and tide forcing but should also consider hydrologic forcing.

Acknowledgements

This research was funded in part under Contract No. W912EP-06-D-0012 from Taylor Engineering, Inc. and the US Army Corps of Engineers (USACE). The statements and conclusions are those of the authors and do not necessarily reflect the views of Taylor Engineering, Inc., USACE, or their affiliates. The authors thank Dingbao Wang, Albert Dai, and Stephen Medeiros for providing reviews of the paper.

References

Arcement, G.J., Schneider, V.R., 1989. Guide for Selecting Manning's Roughness Coefficients for Natural Channels and Floodplains. Water Supply Paper 2339, United States Geological Survey, Tallahassee, Florida.

Ayres Associates, 1999. Nassau River Basin Comprehensive Floodplain Management Study. Special Publication SJ99-SP7, Jacksonville, Florida.

Bacopoulos, P., Funakoshi, Y., Hagen, S.C., Cox, A.T., Cardone, V.J., 2009. The role of meteorological forcing on the St. Johns River (northeastern Florida). J. Hydrol. 369 (1/2), 55–70.

Bacopoulos, P., Parrish, D.M., Hagen, S.C., 2011. Unstructured mesh assessment for tidal model of the South Atlantic Bight and its estuaries. J. Hydraul. Eng. Spec. Iss. Coast. Maritime Hydraul. 49 (4), 487–502.

Bergman, M.J., 1992. Volume 2 of the Lower St. Johns River Basin Reconnaissance: Surface Water Hydrology. Technical Report SJ92-1, St. Johns River Water Management District, Palatka, Florida.

Bunya, S., Dietrich, J.C., Westerink, J.J., Ebersole, B.A., Smith, J.M., Atkinson, J.H., Jensen, R., Resio, D.T., Luettich, R.A., Dawson, C., Cardone, V.J., Cox, A.T., Powell, M.D., Westerink, H.J., Roberts, H.J., 2010. A high-resolution coupled riverine flow, tide, wind, wind wave, and storm surge model for southern Louisiana and Mississippi, I: model development and validation. Mon. Weather Rev. 138 (2), 345–377.

Cardone, V.J., Cox, A.T., Greenwood, J.A., Thompson, E.F., 1994. Upgrade of a Tropical Cyclone Surface Wind Field Model. Miscellaneous Paper CERC-94–14. US Army Corps of Engineers, Washington, DC.

Cox, A.T., Greenwood, J.A., Cardone, V.J., Swail, V.R., 1995. An interactive objective kinematic analysis system. In: Proceedings of the 4th International Workshop on Wave Hindcasting and Forecasting, Banff, Alberta, Canada.

Camp Dresser & McKee Inc., 2007. Final Report of Specific Purpose Aerial Photography and LIDAR Survey, Digital Elevation Model and Contours for Duval County, Florida. Minimum Technical Standards Report for Contract No. 6354-12, City of Jacksonville, Jacksonville, FL.

Dame, R., Alber, M., Allen, D., Mallin, M., Montague, C., Lewitus, A., Chalmers, A., Gardner, R., Gilman, C., Kjerfve, B., Pinckney, J., Smith, N., 2000. Estuaries of the South Atlantic coast of North America: their geographical signatures. Estuaries 23 (6), 793–819.

Dietrich, J.C., Kolar, R.L., Westerink, J.J., 2006. Refinements in continuous Galerkin wetting and drying algorithms. In: Proceedings of the 9th International Conference on Estuarine and Coastal Modeling, Charleston, South Carolina.

Garratt, J.R., 1977. Review of drag coefficients over oceans and continents. Mon. Weather Rev. 105 (7), 915–929.

Hagen, S.C., Zundel, A.K., Kojima, S., 2006. Automatic, unstructured mesh generation for tidal calculations in a large domain. Int. J. Comput. Fluid Dyn. 20 (8), 593–608.

Hagen, S.C., Bacopoulos, P., Cox, A.T., Cardone, V.J., 2011. Hydrodynamics of the 2004 Florida hurricanes. J. Coastal Res. doi:10.2112/JCOASTRES-D-10-00170.1.

Homer, C., Huang, C., Yang, L., Wylie, B., Coan, M., 2004. Development of a 2001 national land-cover database for the United States. Photogramm. Eng. Remote Sens. 70 (7), 829–840.

Kinnmark, I., 1985. The shallow water wave equations: formulation, analysis and application. In: Brebbia, C.A., Orszag, S.A. (Eds.), Lecture Notes in Engineering, vol. 15. Springer, New York, pp. 1–187.

Kolar, R.L., Westerink, J.J., Cantekin, M.E., Blain, C.A., 1994. Aspects of nonlinear simulations using shallow-water models based on the wave continuity equation. Comput. Fluids 23 (3), 523–538.

Le Provost, C., Lyard, F., Molines, J.M., Genco, M.L., Rabilloud, F., 1998. A hydrodynamic ocean tide model improved by assimilating a satellite altimeter-derived data set. J. Geophys. Res. 103 (C3), 5513–5529.

Luettich, R.A., Jr., Westerink, J.J., 2006a. ADCIRC: A Parallel Advanced Circulation Model for Oceanic, Coastal and Estuarine Waters; Users Manual for Version 45.08. <http://adcirc.org/document/ADCIRC_title_page.html>.

Luettich, R.A., Jr., Westerink, J.J., 2006b. Formulation and Numerical Implementation of the 2D/3D ADCIRC Finite Element Model, Version 44.XX. <http://adcirc.org/document/ADCIRC_title_page.html>.

Lynch, D.R., Gray, W.G., 1979. A wave equation model for finite element tidal computations. Comput. Fluids 7 (3), 207–228.

Mattocks, C., Forbes, C., Ran, L., 2006. Design and Implementation of a Real-Time Storm Surge and Flood Forecasting Capability for the State of North Carolina. UNC-CEP Technical Report, University of North Carolina, Chapel Hill, North Carolina.

National Climatic Data Center, 2011. Quality Controlled Local Climatological Data. <http://gis.ncdc.noaa.gov/map/lcd/>.

National Land Cover Data, 2011. Multi-Resolution Land Characteristics Consortium. <http://www.epa.gov/mrlc/nlcd-2006.html>.

National Oceanic and Atmospheric Administration, 2011. National Ocean Service Hydrographic Survey Data. <http://maps.ngdc.noaa.gov/viewers/nos_hydro/>.

National Weather Service, 2011. National Weather Prediction Links. <http://www.srh.noaa.gov/ssd/nwpmodel/html/gfs.htm>.

Powell, M.D., Houston, S.H., Amat, L.R., Morisseau-Leroy, N., 1998. The HRD real-time hurricane wind analysis system. J. Wind Eng. Ind. Aerodyn. 77 (78), 53–64.

Reid, R.O., 1990. Tides and storm surges. In: Herbich, J.B. (Ed.), Handbook of Coastal and Ocean Engineering, I: Wave Phenomena and Coastal Structures. Gulf Publishing Company, Houston, Texas, pp. 533–590.

Sucsy, P.V., Morris, F.W., 2002. Calibration of a Three-Dimensional Circulation and Mixing Model of the Lower St. Johns River. Technical Memorandum, Draft 1.1, St. Johns River Water Management District, Palatka, Florida.

Surfbreak Engineering Sciences, Inc., 2009. Field Measurement Project in Support of the United States Army Corps of Engineers' Jacksonville Harbor Navigation Project, Duval County, Florida. Report Submitted to Taylor Engineering, Inc. and US Army Corps of Engineers, Jacksonville District.

Sweet, W., Zervas, C., Gill, S., 2009. Elevated East Coast Sea Level Anomaly: June–July 2009. NOAA Technical Report NOS CO-OPS 051, National Oceanic and Atmospheric Administration, US Department of Commerce, Silver Spring, Maryland.

Thompson, E.F., Cardone, V.J., 1996. Practical modeling of hurricane surface wind fields. J. Waterway Port Coast. Ocean Eng. 122 (4), 195–205.

Toth, D.J., 1993. Volume 1 of the Lower St. Johns River Basin Reconnaissance: Hydrogeology. Technical Report SJ93-7, St. Johns River Water Management District, Palatka, Florida.

United States Army Corps of Engineers Jacksonville District, 2011. Federally Authorized Channels Maintained by The Corps of Engineers. <http://www.saj.usace.army.mil/Divisions/Operations/Branches/Navigation/HydroSurvey/hydro.php>.

United States Geological Survey, 2010. Water Data for the Nation (USGS Gage Station Identification Number USGS 02246500). <http://waterdata.usgs.gov/nwis>.

Westerink, J.J., Luettich, R.A., Feyen, J.C., Atkinson, J.H., Dawson, C., Roberts, H.J., Powell, M.D., Dunion, J.P., Kubatko, E.J., Pourtaheri, H., 2008. A basin- to channel-scale unstructured grid hurricane storm surge model applied to Southern Louisiana. Mon. Weather Rev. 136 (3), 833–864.